Efficient rotational cooling of a cold beam of barium monofluoride

T Courageux, A Cournol, D Comparat, B Viaris de Lesegno, H Lignier

New Journal of Physics
The open access journal at the forefront of physics

Deutsche Physikalische Gesellschaft DPG IOP Institute of Physics

PAPER • OPEN ACCESS

Efficient rotational cooling of a cold beam of barium monofluoride

To cite this article: T Courageux *et al* 2022 *New J. Phys.* **24** 025007

New Journal of Physics
The open access journal at the forefront of physics

Deutsche Physikalische Gesellschaft DPG
IOP Institute of Physics

Published in partnership with: Deutsche Physikalische Gesellschaft and the Institute of Physics

OPEN ACCESS

RECEIVED
13 October 2021

REVISED
19 December 2021

ACCEPTED FOR PUBLICATION
19 January 2022

PUBLISHED
22 February 2022

PAPER

Efficient rotational cooling of a cold beam of barium monofluoride

T Courageux, A Cournol, D Comparat, B Viaris de Lesegno and H Lignier*

Université Paris-Saclay, CNRS, Laboratoire Aimé Cotton, 91405 Orsay, France
* Author to whom any correspondence should be addressed.

E-mail: hans.lignier@universite-paris-saclay.fr

Keywords: optical pumping, rotational cooling, cold beam, barium monofluoride

Abstract

The ability to cool and trap a large number of molecules is currently a crucial challenge for the implementation of various applications in fundamental physics and cold chemistry. We here present an optical cooling of the internal degrees of freedom which maximizes the number of molecules in a minimum number of rotational states. Our demonstration is achieved on a supersonic beam of barium monofluoride seeded in argon, a process that leads to a rotational temperature $T_{\mathrm{rot}} \approx 12$ K. The rotation is then cooled by our optical pumping to approximately $T_{\mathrm{rot}} \approx 0.8$ K which, compared to the initial rotational distribution, corresponds to an increase of the number of molecules in the lowest rotational state by one order of magnitude. Our method employs two light sources coming from tapered amplifiers. The first source, dedicated to the rotational cooling of molecules occupying the fundamental vibrational level, is optimized thanks to a spectral shaping whose resolution is comparable to the separation of the relevant rotational levels. The second source is used to pump the molecules back to the fundamental vibrational level when they escape from it. This work focuses on the relevant features of these two types of optical pumping.

1. Introduction

For about fifteen years, molecules have been seriously considered as good candidates for the search of symmetry breaking effects, the study of many-body systems and cold chemistry. To favor this exploration, it is advantageous to create cold and even ultra-cold samples of molecules [1]. This task is particularly challenging when the studied molecules are formed at high temperature. This can reach more than 1000 K when molecules are created by laser ablation techniques as it is the case, for example, for YbF, BaF, CaF, SrF or ThO. In current experiments, molecules must be first cooled in a cold beam which relies on two well-known methods: buffer gas cooling at cryogenic temperature or supersonic expansion [2]. The performance of the resulting cold molecular beams is generally assessed according to several criteria such as the propagation speed, the translational temperature, the beam divergence and the number of populated internal states. The brightness is a quantity that gathers these quantities: it expresses the number of molecules in a given internal state per steradian per pulse (or per second). For instance, for a molecule such as BaF + candidate for measurements of the electron electric dipole moment [3] and nuclear spin-dependent parity violation [4, 5] + the brightness of buffer gas cooled beams has been demonstrated to attain 5×10^{10} molecules/sr/pulse [6] + as for similar species such as CaF or SrF [2]. This is typically two orders of magnitude larger than what is obtained with supersonic beams [7]. From cryogenic buffer gas cooling, molecules suitable to laser cooling can even be cooled further: SrF and CaF have been sufficiently decelerated and loaded in a magneto-optical trap [8, 9] and, according to recent advances [10], it may be thought that the same feat is at hand with BaF. However this might be difficult because BaF has a larger mass and less favorable optical cycling properties than the two other molecules [11]. In any case, whatever is the species, the manipulation of molecular beams encounters strong limitations concerning the yield of molecules. Therefore, any method increasing the brightness is desirable. One possibility is to form more

molecules initially, as in [12] where laser-induced chemistry allows the authors to get a production enhancement by one order of magnitude. Another one is to reduce the beam divergence, i.e. manipulate the molecules such that they move closer to the beam axis. This may be done by transverse laser cooling or guiding [13, 14]. Finally, it may be envisaged to increase the number of molecules per internal state which is the object of the present article.

Our approach consists in cooling the internal degrees of freedom thanks to an optical pumping scheme employing broadband light sources. This method has been successfully applied to several neutral and ionic diatomic molecules [15–19] and could be easily extended to many other species, especially if they feature high vibrational branching ratios and are thus good candidates for laser cooling. As it is well established now, this is the case for alkaline earth monofluorides and monohydroxides [20]. It must be emphasized that high vibrational branching ratios favor optical pumping but are not a necessary condition. In fact, the internal cooling of molecules, such as NaCs and Cs_2 [16, 17], has been achieved despite the absence of this advantageous property.

In a previous work, we already demonstrated that a supersonic beam of BaF could be optically pumped to enhance the population per rovibrational state [18]. In this way, we succeeded to lower the rotational temperature, initially at 50 K, to roughly 6 K. Thanks to the development of suitable light sources, we here demonstrate that this technique can be significantly improved: we are now able to obtain a rotational temperature of about 0.8 K. This is better than what is observed in the state-of-the-art cold BaF sources: in the buffer gas experiment reported in [6] and in the optimized supersonic experiment reported in [7] the rotational temperature was found to be 7.1 and 3.5 K respectively.

This article is organized in three main sections. In the first one, we briefly describe the main elements of the experiment, namely the supersonic beam, the two light sources used for optical pumping and the detection based on resonance enhanced multi-photon ionization (REMPI). Our rotational pumping scheme is based on the excitation of rovibronic transitions from the vibrational ground state. However, this process induces a transfer of molecules in the first excited vibrational state where rotational pumping is not active. Therefore, as it will be described in the second section, our experience requires an optical source to pump all the molecules from the first vibrational state to the ground state. We show that the measured pumping rate is found to be in good agreement with a rate equation model. Finally, in the third and last section, the action of rotational pumping is studied from our REMPI spectra. Their fitting by numerical methods allows us to reconstruct a rotational distribution whose fine characteristics are discussed. We finally show that our results are well reproduced by a numerical simulation of the rotational pumping.

2. Experimental overview

Our experiment set-up is outlined in figure 1. It relies on an adiabatic expansion of Ar with 2% of SF_6 from a high pressure reservoir (5 bar) to a vacuum chamber through a pulsed general valve opening at a rate of 10 Hz. The vacuum chamber is made of an expansion chamber where the working pressure is $\sim 10^{-5}$ mbar, connected, through a 3 mm skimmer, to an experiment chamber where the pressure does not exceed 3×10^{-7} mbar. In the expansion chamber, near the valve aperture, BaF molecules are formed through a chemical reaction between SF_6 molecules and Ba atoms ablated from a solid target with a focused pulsed YAG laser at 532 nm (25 mJ). Because the ablation releases a high amount of energy, BaF molecules initially move fast and have much energy in their internal degrees of freedom. Once formed, they undergo a partial thermalization through collisions with the argon atoms. This leads to rotational and translational temperatures that are generally one or two orders of magnitudes lower than the vibrational temperature. In our set-up, we measured a vibrational temperature as high as 2100 K [21] while the rotational temperature is in the range 10–100 K [18]. The translational temperature has not been determined but is expected to be lower than or similar to the rotational temperature [22]. The cooling performance is crucially dependent on the relative positions of the valve and the ablation spot but also on a proper timing between the valve opening and the ablation pulse triggering. Some of the cooled BaF molecules are entrained in the flow of argon and penetrate the experiment chamber where they propagate freely, i.e. experience a marginal number of collisions. Only the molecules passing through a hole drilled in a glass plate (2.5 mm diameter) placed 250 mm downward from the skimmer, are submitted to the optical pumping implemented in this work.

The BaF molecules lying in the ground electronic state $X^2\Sigma$ are submitted to our rotational cooling scheme that employs two light beams aligned on the molecular beam axis. These light beams are issued from two tapered amplifiers and address two different rovibrational transitions (see figure 2). The light at ~ 859 nm is tuned on transitions $X^2\Sigma(v'' = 0, J'', N'') \rightarrow A^2\Pi_{1/2}(v' = 0, J')$, where v'' and v' are vibrational quantum numbers, J'' and J' are total angular momenta and N'', only relevant for the X state, is the total angular momentum apart from spin (throughout the article, primes refer to the quantum numbers of any

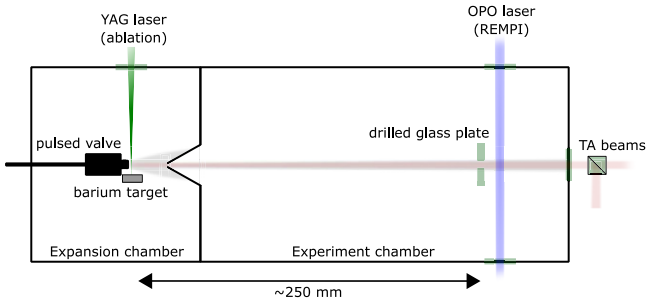

Figure 1. Schematics of the experimental set-up. A supersonic beam of BaF is irradiated by up to two light TA beams for vibrational and rotational pumping (see main text and figure 3 for details). The REMPI detection is achieved by an OPO laser and multichannel plates (not depicted).

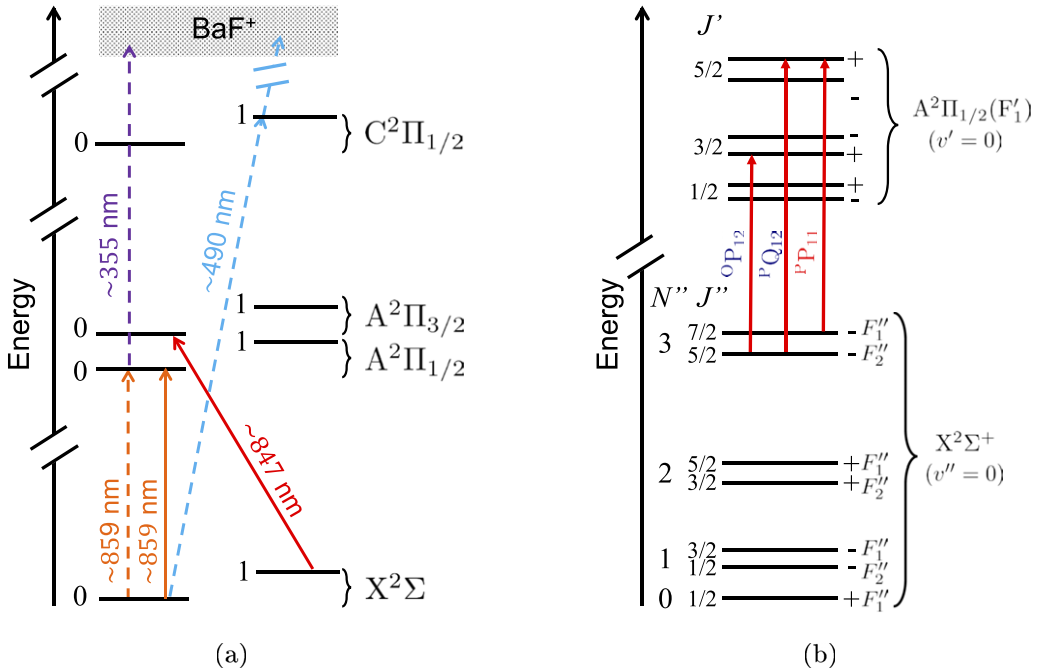

Figure 2. (a) Simplified diagram of BaF vibrational levels and transitions addressed by the different laser sources used in this work (see main text for the spectroscopic notations). The lowest vibrational levels of the four relevant electronic states are represented by horizontal black segments with, next to them, the corresponding vibrational quantum number 0 and 1. The solid line arrows refer to continuous broadband light sources used for optical pumping: the transitions at $\sim$ 847 and $\sim$ 859 nm are dedicated to vibrational and rotational pumping respectively. The dashed line arrows indicate pulsed laser sources used for REMPI detection: the ionization through the C state uses two identical photons at $\sim$ 490 nm while the ionization through the A state requires two different photons at $\sim$ 859 and 355 nm. (b) Energy diagram of the first rotational levels of $X^2\Sigma(v'' = 0)$ and $A^2\Pi_{1/2}(v' = 0)$. The light source used for rotational pumping is used to excite $^{O}P_{12}$, $^{P}P_{11}$ and $^{P}Q_{12}$ transitions indicated by the arrows for $N'' = 3$ only (the same is true for $1 \leqslant N'' \lesssim 15$).

excited state and double primes to those of the ground state). It is used to pump the molecules toward the low values of J'' and N''. The fluorescence cycles resulting of this light–matter interaction induces a possible decay to $v'' = 1$. To counteract this effect, a vibrational pumping is set to transfer the molecules back to $v'' = 0$. This role is held by the second light beam whose wavelength at $\sim$ 847 nm addresses the transitions $X^2\Sigma(v'' = 1, J'', N'') \rightarrow A^2\Pi_{3/2}(v' = 0, J')$. Two acousto-optic modulators allow us to choose the duration of the interaction which is at most 440 μs. This time limitation is imposed by the beam velocity of $\sim$ 580 m s^{-1} in the experiment chamber.

The detection relies on the REMPI technique ensured by a tunable pulsed laser (Continuum Sunlite EX OPO) based on an optical parametric oscillator (OPO). In this process, molecules are first excited to an intermediate state from which they are subsequently ionized, as shown in figure 2(a). The resulting ions are finally detected by a stack of two microchannel plates (MCP). Photo-ionization spectra are easily obtained by measuring the MCP signal with respect to the OPO wavelength. These spectra are essentially structured by the resonant transitions between the X state and the intermediate state. They feature vibrational bands where some of the rovibrational lines are resolved if the pulse energy is sufficiently low. With a pulse energy

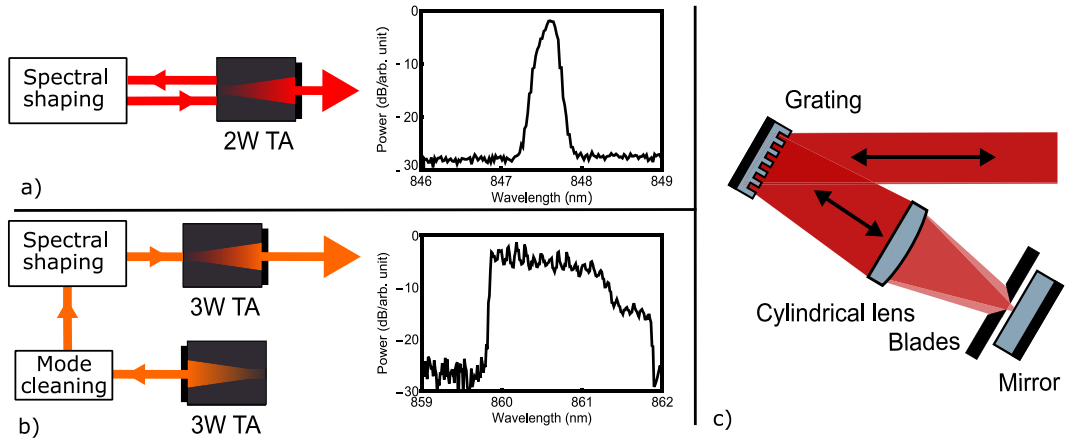

Figure 3. Schematic diagrams of optical sources using tapered amplifiers and typical examples of generated optical spectra recorded with our OSA for (a) vibrational pumping and (b) rotational pumping. The spectral shaping used in (a) and (b) is based on the folded 4-f line in the drawing (c). In (a), the spectrum shows a cut-off resolution of about 2.8 cm^{-1} (0.2 nm) while, in (b) the spectrum features an optimized cut-off resolution of 0.28 cm^{-1} (0.02 nm). (c) The incoming light beam is filtered after a round trip in a folded 4-f line: the light dispersed by the grating goes through a cylindrical lens and is reflected back by a mirror with a mask made of two blackened blades. Only the spectral components of the light passing through the aperture between the blades are selected and recombined by the grating. The 4-f line acts as a pass-band filter whose center and width are adjusted by the blade positions.

of 50 μJ and a typical beam surface of 0.25 cm^2, the width of the resolved rovibrational lines is similar to the OPO linewidth (0.1 cm^{-1}). When working with higher energy pulses, power broadening effects come into play and can be so strong that no rovibrational lines can be distinguished [21].

3. Vibrational pumping

3.1. Principles

As mentioned previously, the vibrational pumping is necessary to prevent an accumulation of molecules in $v'' = 1$ induced by the rotational pumping. We chose to excite the transitions $X^2\Sigma(v'' = 1, J'', N'') \rightarrow A^2\Pi_{3/2}(v' = 0, J')$ because molecules excited into $v' = 0$ decay toward $v'' = 0$ with a probability of 0.95 corresponding to the Franck–Condon factor between $v' = 0$ and $v'' = 0$. In order to excite all the molecules in $v'' = 1$, the light spectrum must contain the suitable frequencies to excite all the J'' values that are significantly populated. In this work, as it will be seen further, the rotational temperature obtained with our adiabatic expansion is $T_{rot} \approx 12$ K. This means that the molecules are roughly spread over the 15 lowest values of J''. Our strategy has consisted in using a broadband laser covering the Q-branch transitions ($\Delta J = J' - J'' = 0$) which requires a width of the light spectrum of about 4 cm^{-1}.

3.2. Description of the optical sources and transitions

The broadband light source is based on a 2 W TA (Eagleyard 2 W EYP-TPA-0850) seeded by its own spontaneous emission (SE). As explained in our previous works [18], the SE is sent into a folded 4-f line [23], i.e. a pass-band filter as described in figures 3(a) and (c). The filter is set to create a 4.2 cm^{-1}(0.3 nm) band centered on 117 96.7 cm^{-1} (847.6 nm). In this configuration, the TA output power is about 1.6 W but, due to usual losses in the optical line, the effective power available in the experiment chamber is $P = 1.1$ W. As the diffraction properties of the TA output light are close to a that of Gaussian beam (the TA beam quality factor $M^2 \lesssim 2$), the beam is easily collimated with a typical 3 mm waist over the length of the experiment chamber (25 cm). It is aligned with the 2.5 mm hole made in the glass plate and the skimmer. To ensure a good overlap with the molecular beam, the alignment was optimized by maximizing the depletion signal of $v'' = 1$. This depletion was measured via REMPI by tuning the OPO wavelength to 20 427 cm^{-1} which corresponds to the Q-branch transitions $X^2\Sigma(v'' = 1, J'', N'') \rightarrow C^2\Pi_{3/2}(v' = 0, J')$. By scanning the OPO laser in the range 20 350 + 20 450 cm^{-1}, the REMPI technique was also used to record spectra where the vibrational bands can be clearly distinguished. For these measurement, the OPO energy was purposely set at 1 mJ to cause power broadening. In this way, the maximum of the Q branch results from the simultaneous ionization of many rotational levels (J'', N'').

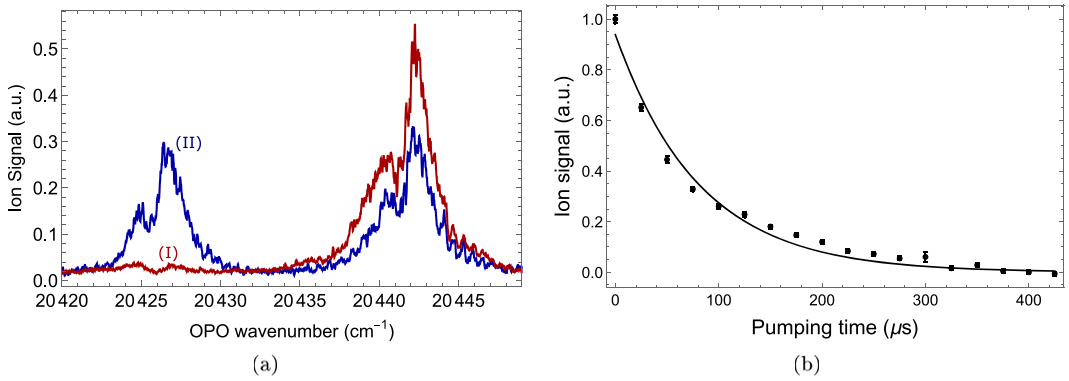

Figure 4. Vibrational pumping from $v'' = 1$ to $v'' = 0$. (a) Two REMPI spectra taken with (I) + (red line) and without (II) + (blue line) vibrational pumping. The spectral region scanned by the OPO laser shows the vibrational bands $v'' = 0$ ($\sim 20\,442$ cm^{-1}) and $v'' = 1$ ($\sim 20\,427$ cm^{-1}). (b) Depletion of the ion signal in $v'' = 1$ versus the time of application of the vibrational pumping. The data (dots) result of an REMPI detection at $20\,443$ cm^{-1} which corresponds to an ionization through the Q-branch peak of the resonant transition $X^2\Sigma(v'' = 1, J'', N'') \rightarrow C^2\Pi_{3/2}(v' = 0, J')$ (see main text for the spectroscopic notations). The black line is an exponential fit of the data that gives a time constant of $\tau_{exp} = 81$ μs.

3.3. Results and discussion

We now present our results related to the vibrational pumping. In figure 4(a), we present two REMPI spectra taken with and without vibrational pumping where the vibrational bands $v'' = 0$ and $v'' = 1$ are visible. In absence of pumping, the spectrum shows a similar REMPI signal for $v'' = 0$ and $v'' = 1$. The second spectrum, obtained with vibrational pumping applied during all the propagation duration of the molecular beam, shows drastic modifications: the signal for $v'' = 1$ has disappeared almost entirely while that for $v'' = 0$ increased. The signal in the vibrational levels $v'' \geqslant 2$ (not shown here) are almost unaffected by the vibrational pumping. From these results, it is then obvious that there is a population transfer from $v'' = 1$ to $v'' = 0$ that is almost exclusive as expected. Following our previous analysis in [21], the relative increase of the peak in $v'' = 0$ caused by the pumping gives a rough estimate of the vibrational temperature although the thermalization of the vibration is not fully achieved. The observed increase of about 60% corresponds to a temperature of about 2000 K if we make the assumption that the vibrational distribution follows a Maxwell distribution.

We now present the experimental determination of the vibrational pumping rate. It consists in measuring the evolution of the depletion signal of $v' = 1$ with respect to the time during which the light source is applied. A typical result is displayed in figure 4. By fitting these data with a decreasing exponential function, we find a time constant $\tau_{exp} = 81$ μs whose inverse can be interpreted as the pumping rate from $v'' = 1$ to $v'' = 0$. It is then possible to compare τ_{exp} to the time given by a simple model. In fact, as the molecules excited to $v' = 1$ essentially decay to $v'' = 0$, we expect that this time be roughly the same as the excitation time induced by our broadband source which is estimated by

$$\tau_{th} = \frac{c}{B_e^{\nu}\bar{I}_{\nu}}, \tag{1}$$

where c is the speed of light, $\bar{I}_{\nu}$ is the average spectral intensity in W m^{-2} Hz^{-1}) and

$$B_e^{\nu} = \frac{3\lambda^3}{32\pi^2\hbar}\Gamma\alpha, \tag{2}$$

is a typical Einstein coefficient for the rovibrational transitions excited by the TA. Its calculation requires the wavelength $\lambda \approx 847$ nm of the transitions $X^2\Sigma(v'' = 1, J'', N'') \rightarrow A^2\Pi_{3/2}(v' = 0, J')$, the natural width of the excited state $\Gamma \approx 2\pi \times 3.32$ MHz [24] and α, a coefficient accounting for the Q-branch transitions. More precisely, $\alpha = q_{01} \times$ HL where $q_{01} \approx 0.036$ is the Franck–Condon factor between $v'' = 0$ and $v' = 1$ calculated from the Morse potentials of the A and X states thanks to the parameters found in [25] and HL ≈ 0.27 is an averaged value of the Hönl–London coefficients for the Q-branch A–X transitions that we calculated with the PGOPHER software [26]. This allows us to estimate $B_e^{\nu} \approx 1.1 \times 10^{19}$ m^3 Hz (J^{-1} s^{-1}). The mean spectral intensity $\bar{I}_{\nu}$ is obtained by dividing the mean light intensity $\bar{I}$ by the TA typical spectral width (4.3 cm^{-1}). The averaged intensity seen by the molecules is given by $\bar{I} = 4P\{1 - \exp[-D^2/(2w^2)]\}/(\pi D^2)$ where $w \approx 3$ mm is the beam waist and $D = 2.5$ mm is the hole diameter. This results in $\bar{I}_{\nu} \approx 0.5$ μW m^{-2} Hz^{-1}. Eventually, we obtain from equation (1) $\tau_{th} \approx 53$ μs, a time slightly smaller than the experimental time constant τ_{exp}. The time difference could certainly be explained by the

approximate nature of our model. In any case, the same order of magnitude is found, which allows us to conclude that the vibrational pumping works as expected.

Importantly, we note that the transfer of molecules from $v'' = 1$ to $v'' = 0$ requires a time that is about 5.5 times shorter than the propagation time of the molecular beam. The rotational pumping described below makes use of a light source with a similar spectral power density as the vibrational pumping source. Because of the difference between Franck–Condon factors, the ratio between the strengths of the rotational pumping transitions $(v'' = 0) \rightarrow (v' = 0)$ and the vibrational pumping transitions $(v'' = 1) \rightarrow (v' = 0)$ is about 20. Hence the typical absorption time through rotational pumping must be 20 times shorter than τ_{exp}. On the other hand, as the probability for a decay $(v' = 0) \rightarrow (v'' = 1)$ is slightly lower than 0.05, the decay of molecules to $(v'' = 1)$ induced by rotational pumping is typically achieved after 20 absorption–emission cycles. As a result, the typical time for molecules to be transferred from $v'' = 0$ to $v'' = 1$ is equivalent to τ_{exp}. Finally, if we consider that a time $2\tau_{\mathrm{exp}}$ is needed to achieve 20 fluorescence cycles on $(v'' = 0) \rightarrow (v' = 0)$ to repump molecules from $v'' = 1$ to $v'' = 0$, we may estimate that, over all the beam propagation time (440 μs), the molecules undergo about 55 fluorescence cycles.

4. Rotational pumping

4.1. Principles

To understand how rotational pumping works, it is important to consider the role of the selection rules related to the dipole electric transition. Two of them are particularly important: the first one is the change of parity $(+ \leftrightarrow -)$ while the second is the change of angular momentum $\Delta J = J' - J'' = -1, 0, +1$, giving rise to the three series of excitation lines called, respectively, P, Q, R branches. For the A–X transitions, the description is actually a more complex pattern of lines where six branches can be identified. This comes from the fact that the X state is well described by the Hund's case (b) for which $N'' = J'' - S''$, where S'' is the electronic spin, is a good quantum number. Hence, two values of J'' are possible for each value of N'' (except for $N'' = 0$ where only one value exists), namely $J'' = N'' + 1/2$ and $J'' = N'' - 1/2$, the so-called spin components referred to as F_1'' and F_2''. On the other hand, the A state belongs to Hund's case (a) for which a quantum number equivalent to a total angular momentum apart from spin cannot be defined. Instead, the relative orientation of the total electronic spin and the total electronic orbital momentum gives rise to the doublet components $A^2\Pi_{1/2}$ and $A^2\Pi_{3/2}$ where the rotational energy terms are denoted F_1' and F_2' respectively. It is common to use the quantity $\Delta N = N' - N''$ (where $N' = J' - 1/2$ and $N' = J' - 3/2$ for the transitions to $A^2\Pi_{1/2}$ and $A^2\Pi_{3/2}$ respectively) and to name the branches with the notation ${}^{\Delta N}\Delta J_{F'F''}(J'')$, with the subscripts F' and F'' referring to one of the doublet components of the upper and lower states. For the transitions $X^2\Sigma(v'' = 0, J'', N'') \rightarrow A^2\Pi_{1/2}(v' = 0, J')$ involved in rotational pumping, it is possible to find transitions with the subscript $\Delta N = -2, -1, 0, 1$ labeled O, P, Q, R giving rise to the six branches ${}^{\mathrm{O}}\mathrm{P}_{12}$, ${}^{\mathrm{P}}\mathrm{P}_{11}$, ${}^{\mathrm{P}}\mathrm{Q}_{12}$, ${}^{\mathrm{Q}}\mathrm{Q}_{11}$, ${}^{\mathrm{Q}}\mathrm{R}_{12}$, ${}^{\mathrm{R}}\mathrm{R}_{11}$ shown in the Fortrat diagram in figure 5. We stress the fact that each branch excites one of the two doublet components: the states belonging to the F_1'' component can be excited by the branches ${}^{\mathrm{P}}\mathrm{P}_{11}$, ${}^{\mathrm{Q}}\mathrm{Q}_{11}$, ${}^{\mathrm{R}}\mathrm{R}_{11}$, and the F_2'' by the remaining branches. Note that a molecule is not definitely assigned to a given spin component as the latter can be changed through SE.

The scheme of our rotational pumping relies on a cycle of absorption and SE that statistically decreases the angular momenta J'' and N''. This can be achieved by driving $\Delta J = -1$ excitations toward $A^2\Pi_{1/2}$ after which the SE causes another change $\Delta J = 0, \pm 1$. For our purpose, it is mandatory to excite both ${}^{\mathrm{P}}\mathrm{P}_{11}$ and ${}^{\mathrm{O}}\mathrm{P}_{12}$ in order to address transitions from the two doublet components, see example in figure 2(b). In fact, the excitation of a single branch would transfer all the molecules in one of the two components where they could not be excited any more. For the two branches, there are three possible decay paths, namely ${}^{\mathrm{P}}\mathrm{P}_{11}$, ${}^{\mathrm{P}}\mathrm{Q}_{12}$, ${}^{\mathrm{R}}\mathrm{R}_{11}$ and ${}^{\mathrm{O}}\mathrm{P}_{12}$, ${}^{\mathrm{Q}}\mathrm{Q}_{11}$, ${}^{\mathrm{Q}}\mathrm{R}_{12}$ for an excitation using the branches ${}^{\mathrm{P}}\mathrm{P}_{11}$ and ${}^{\mathrm{O}}\mathrm{P}_{12}$ respectively. As a consequence, a single cycle of fluorescence is likely to decrease N'' and J'' by up to two units of angular momentum; the less favorable decay corresponding to a return to the starting state (then N'' and J'' are unchanged). By repeating this process a sufficient number of times, molecules are expected to accumulate, at best, in the two states of lowest energy with opposite parities, namely $(N'' = 0, J'' = 1/2, +)$ and $(N'' = 1'', J = 1/2, -)$. In fact, the parity of molecules in the X state cannot be modified by any fluorescence cycle involving two electric dipole transitions.

Experimentally, the excitation of ${}^{\mathrm{P}}\mathrm{P}_{11}$ and ${}^{\mathrm{O}}\mathrm{P}_{12}$ branches can be achieved by a light spectrum with a band shape covering all the lines corresponding to the states J'' that are significantly populated at the rotational temperature of the molecular beam. As mentioned previously, the molecules populate the levels up to $N'' \approx 15$. This implies that the pass-band must range from $\sim 11\,620$ to $\sim 11\,629$ cm^{-1}. The blue cut-off frequency plays an important role here: it is tuned to a value for which the lowest rotational levels cannot be excited by the light spectrum.

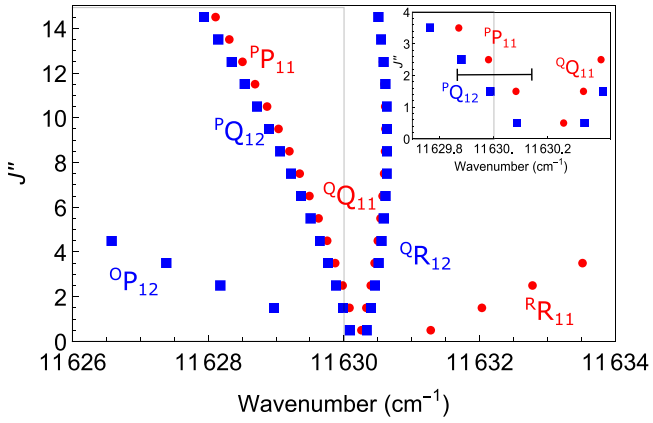

Figure 5. Fortrat Diagram for the transitions $X^2\Sigma(v''=0,J'',N'') \rightarrow A^2\Pi_{1/2}(v'=0,J')$. The transitions from both components F_1'' and F_2'' of the X state are indicated by red circles and blue squares respectively. The branches $^{P}P_{11}$ and $^{P}Q_{12}$ almost overlap, and the same goes for the branches $^{Q}Q_{11}$ and $^{Q}R_{12}$. The hatched part corresponds to the spectral range covered by the excitation light used for rotational pumping (the red cut-off frequency at ∼11 620 cm^{-1} is not visible). Inset: zoom in around the blue cut-off frequency at 11 630 cm^{-1} showing that the $J''=3/2\,(F_2'')$, $5/2\,(F_1'')$ from $N''=2$ are the lowest states pumped by $^{P}Q_{12}$ and $^{P}P_{11}$ respectively. The horizontal black segment indicates the cut-off spectral resolution (0.27 cm^{-1}) given in the main text.

According to the Fortrat diagram in figure 5, the intended light spectrum (hatched area) is also capable to excite the F_2'' component by the $^{P}Q_{12}$ branch. This might seem problematic given that it may increase J'' but a careful analysis shows it is not. In fact, after a fluorescence cycle, this branch can lead, at worse, to an unwanted increase of the J'' value by one unit of angular momentum while the N'' value is kept unchanged. Necessarily this implies a component change from F_2'' to F_1'' from which the excitation by the $^{P}Q_{12}$ branch cannot occur once more. The only possibility for a subsequent excitation therefore relies on the $^{P}P_{12}$ branch where J'' and N'' can finally decrease. Another concern would be an excitation by the $^{Q}Q_{11}$ and $^{Q}R_{12}$. However, our light spectrum covers the lines for $J'' \gtrsim 20$ only which cannot impact our molecules with their initial rotational distribution at $T_{rot} = 12$ K.

4.2. Description of the optical sources and transitions

The broadband light source developed for rotational pumping shares similar features with the source used for vibrational pumping. Nevertheless it does not employ a self-injected TA as used for vibrational pumping but a TA injected by an external seed as sketched in figure 3(b). This solution was necessary to get rid of instabilities that appeared with the 3 W TA model (DILAS TA-0850-3000-DHP) used for rotation, different from the 2 W TA dedicated to the vibration. The light source providing the seed comes from the SE delivered by a second 3 W TA, which has several advantages compared to other possible seed sources with a broadband spectrum such as a LED or a broadband diode laser. By operating the second TA at a sufficiently low injection current, its output power is about 200 mW, its spectrum extends smoothly over ∼ 5 nm and the good propagation properties ($M^2 \approx 1.5$) facilitates the injection of the first TA. Before its amplification, this light beam makes a round trip in a similar folded 4-f line to the one used for the vibration pumping source. Prior to the 4-f line, the spatial mode of the beam is filtered by focusing it onto a 60 μm pinhole, which leads to a power loss of 40%. This operation aims at recovering a beam with an almost perfectly Gaussian mode ($M^2 = 1$) which helps to optimize the spectral filtering resolution. As a result, the spectral resolution, characterized by the edge steepness, i.e. the spectral region over which a cut-off blocks 10%–90% of the signal power, is about 0.02 nm (8 GHz or 0.27 cm^{-1}). Compared to our previous work where the light source was a 7 W broadband diode laser, the cut-off resolution has been improved by a factor 17 [18]. After spectral shaping, the seed (∼30 mW) is amplified and the resulting useful power is as high as 1.7 W. The output beam is finally combined with the light beam used for vibrational pumping through a polarizing beamsplitter cube (see figure 1). For rotational cooling, the two light sources are applied simultaneously during the time of the beam propagation. When we tried to apply the rotational cooling only, we observed a decrease of the signal in $v''=0$ that was correlated to an increase of the signal in $v''=1$. In this case, after roughly 100 μs, the signal $v''=0$ has almost completely disappeared.

In order to analyze the effect of rotational pumping, it is necessary to measure a spectrum for molecules in $v''=0$ from which we must be able to extract reliable information about the rotational populations. With the REMPI detection scheme using the C state, as used to characterize the vibrational pumping, we usually encountered a congestion of lines, especially for those corresponding to the lowest values of J'' and

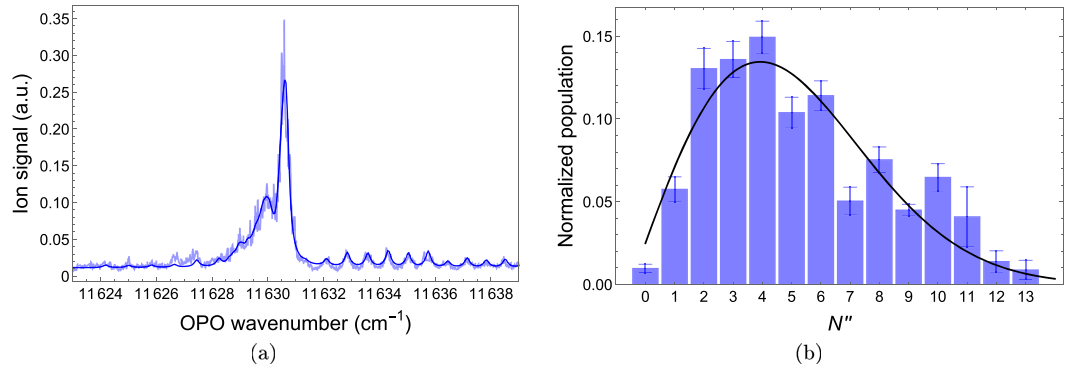

Figure 6. (a) Experimental REMPI spectrum obtained after vibrational pumping and its fitting curve (blue line) (see main text for details). (b) Bar chart of the normalized rotational distribution resulting from the spectrum fit and its fit by a Maxwell–Boltzmann (M–B) function (black line). The rotational temperature given by the M–B fit is $T_{\mathrm{rot}} \approx 12$ K.

N'' [18, 21]. To facilitate our population analysis, we thus chose another REMPI scheme for which the separation between the rotational lines is as large as possible, cf figure 2(a). This REMPI relies on the resonant transitions $X^2\Sigma(v''=0,J'',N'') \rightarrow A^2\Pi_{1/2}(v'=0,J')$ that can be excited by our OPO laser and on an ionization step ensured by the OPO pump pulsed laser at 355 nm. The use of this UV laser is necessary because the energy difference between the A state and the ionization threshold is much larger than the OPO photon energy. In addition to its use to record rotational spectra of the X–A (0–0) band, the REMPI detection was also employed to optimize our optical pumping to low rotational levels. To do so, the OPO was tuned to excite the lowest rotational states ($J''=1/2$ or $J''=3/2$) and the resulting REMPI signal was maximized by adjusting the blue cut-off frequencies of the rotational source. According to a measurement performed with an optical spectrum analyzer Ando AQ6317b (OSA), the maximum signal was obtained with a blue cut-off at $11\,630 \pm 0.02$ cm^{-1}, the uncertainty coming from the OSA accuracy. This value must be compared to lowest rotational transitions shown in the inset of figure 5, namely $^{P}P_{11}(5/2)$ and $^{P}Q_{12}(3/2)$ expected at 116 29.98 cm^{-1} and 116 29.99 cm^{-1} respectively and $^{Q}P_{11}(3/2)$ and $^{Q}Q_{12}(1/2)$ expected at 116 30.08 cm^{-1} and 116 29.09 cm^{-1} (note that for $J''=1/2$, the transition is of type $^{Q}Q_{12}$ and not $^{P}Q_{12}$ as it is for $J''>1/2$).

4.3. Results and discussion

The effect of our rotational pumping is analyzed through the determination of the rotational distribution. This tasks consists in fitting the REMPI spectra with a numerical function which, in short, is a sum of the lines corresponding to transitions $X^2\Sigma(v''=0,J'',N'') \rightarrow A^2\Pi_{1/2}(v'=0,J')$. This approach considers, as in other studies [27, 28],that the ion yield is essentially modulated by the resonant step of the REMPI process. The line parameters, such as their frequency positions and the Hönl–London factors, are directly calculated by the software PGOPHER [26] feeded by the accurate experimental constants found in [29]. Essentially, the fitting procedure is an adjustment of the rotational populations lying in the states $X^2\Sigma(v=0,J'',N'')$ and an adjustment of the line widths (power broadening effects are taken into account). In order to obtain the most reliable distributions, we explored several strategies: either we fitted the whole REMPI spectrum, or we performed a two-step fit. The first step fits the least congested branch only, i.e. $^{R}R_{11}$ in figures 6(a) and 7(a) while the second step fits the rest of the spectrum. Although both methods gave similar distributions, the two-step fit seems to be more relevant regarding the parity aspects + this point will be discussed further. Therefore the results presented here correspond to the two-step procedure. The fitted experimental spectra and the corresponding rotational distributions are shown in figures 6 and 7. Note that the rotational distributions are also fitted by a M–B function which is characterized by a rotational temperature T_{rot}.

When the vibrational pumping transferring the population from $v''=1$ to $v''=0$ was switched on and the rotational pumping was off, we obtained the REMPI spectrum shown in figure 6(a). As explained in [21], molecules in $v''=1$ and $v''=0$ have a similar rotational distribution and the transfer from $v''=1$ to $v''=0$ induced by the vibrational pumping does not modify it significantly. The distribution resulting from our fitting procedure is shown in figure 6(b) and is associated with an M–B function with $T_{\mathrm{rot}} \approx 12$ K. Note that the error bars only correspond to the least-squares optimization and does not account for the fluctuations of the REMPI signal. In fact, the reconstructed distribution slightly changes from one data set to another, which possibly explains the deviation between our fitted distribution and the M–B function. Besides, at this temperature, the number of populated states is already sufficiently important to cause a

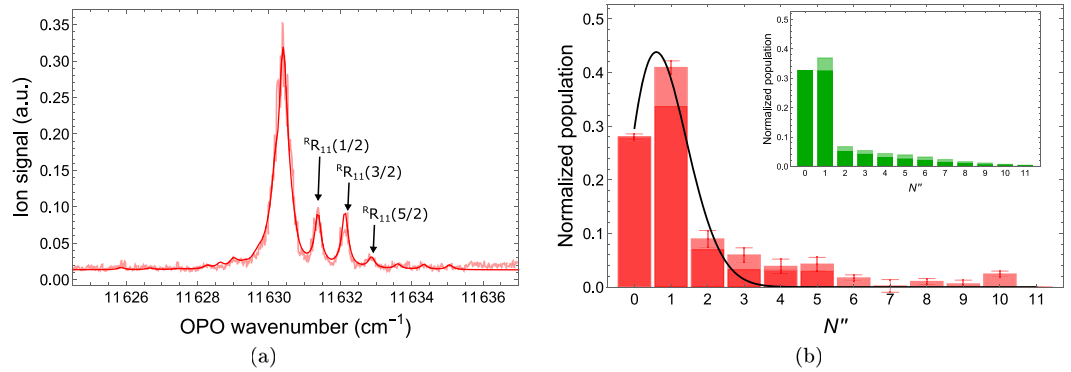

Figure 7. (a) Experimental REMPI spectrum obtained with vibrational pumping and rotational cooling and its fitting curve (red line). The most intense peak results of the unresolved photoionization of several rotational states through the branches $^{P}P_{11}$ and $^{Q}Q_{11}$. (b) Bar chart of the normalized rotational distribution (red bars) resulting from the spectrum fit and its fit by a M–B function (black line). The rotational temperature given by the M–B fit is $T_{rot} \approx 0.8$ K. The top value of a rectangular bar, associated with a statistical error bar, corresponds to the total population in N'' while the darker part of each bar indicates the portion of the F_1'' population. Inset: normalized rotational distribution obtained by numerical simulation of the rotational pumping (see text for details).

congestion of the lines related to branches $^{P}P_{11}$, $^{P}Q_{12}$, $^{Q}Q_{11}$ and $^{R}Q_{12}$. This undoubtedly undermines the fit quality, especially for the low rotational states and the states of the F_2'' component. We think that this congestion is sufficient to explain why the populations of each component for $N'' > 0$ are potentially very different while they are expected to be nearly equal when starting from an M–B distribution. This expectation can be implemented as a constraint in the fit: by doing so, the spectrum remains well fitted and the rotational distribution is still characterized by $T_{rot} \approx 12$ K. We can thus consider that our fitting procedure allows us to reasonably determine the rotational distribution even though the state population is subjected to a non-negligible uncertainty.

We now examine the situation where the light source of rotational pumping was added to the vibrational pumping. In this case, the REMPI spectrum in figure 7(a) was found to be very different from that in figure 6(a). Apart from the most intense peak where a few lines overlap, three individual $^{R}R_{11}(J'')$ lines can now be clearly distinguished and immediately identified: they reveal an important increase of populations in the states $(N'', J'') = (0, 1/2), (1, 3/2)$ and $(2, 5/2)$. The two-step fit provides the rotational distribution also shown in figure 7(b). We clearly see that a roughly 70% of the molecules are now in $N'' = 0$ and $N'' = 1$ which is consistent with the blue cut-off determined previously. The M–B fit of this distribution gives $T_{rot} \approx 0.8$ K, a temperature that must be considered as indicative given that the rotational pumping is not a thermalization process. Beyond the question of the distribution shape, the inadequacy of the M–B distribution has another consequence: the two spin components (for $N'' > 0$) are not expected to have similar populations. In fact, as shown in figure 7, the molecules are essentially distributed in states belonging to the spin component F_1'' (about 80% of the total number of molecules). This affirmation is consistent with a rapid inspection of the REMPI spectrum: the well separated lines of the $^{O}P_{12}$ branch are characterized by very weak intensities. We also verified that the distribution obtained by the fit is in agreement with the preservation of the total populations associated with the two possible parities $(+/-)$. The ratio of this $+/-$ populations is expected to be nearly equal to one as found for an M–B distribution at sufficiently high rotational temperature, which is valid for $T_{rot} \approx 12$ K in absence of rotational pumping. From the experimental distribution, we found this value to be 1.05, which supports the validity of our reconstruction.

We now discuss some generalities regarding the rotational pumping. First of all, by comparing the total population with and without rotational pumping, we found that the rotational pumping induces less than 10% of population loss, which is comparable to the uncertainty over the total population. Nevertheless, part of these losses can be explained by a well-identified mechanism, namely the incomplete repumping of the molecules that decayed to $v'' = 1$ (the relaxation toward $v'' = 2$ being negligible). Next, one may ask whether the rotational pumping modified the distribution as it could be expected. The net accumulation in $N'' = 0$ and $N'' = 1$ was anticipated as it corresponds to the preservation of parity. On the other hand, the mechanism behind the preferential pumping toward the F_1'' component is not trivial.

In order to have a better understanding of our rotational pumping, we simulated it by a full 3D Monte–Carlo model based on rate equations [30]. The key parameters, i.e. the strengths of the optical rovibrational transitions, were determined, as for the fit, by PGOPHER [26] with the experimental data in [29]. Also we used the experimental parameters of the molecular beam (velocity, divergence) and those of

the light source used for rotational pumping (light intensity, spectrum, polarization, cut-off frequency) given above. However, we simplified the transition scheme by neglecting the leakage out of $(v'' = 0) \leftrightarrow (v' = 0)$ which allowed us to avoid the simulation of the vibrational pumping. Thereby we assumed that vibrational pumping does not modify the redistribution of rotational populations in $v'' = 0$. This assumption is legitimate since on average there are 20 times more fluorescence cycles related to rotational pumping than to vibrational pumping.

The result of our simulation with a cut-off at 116 30.05 cm^{-1} is the distribution shown in the inset of figure 7. Clearly, the experience is well reproduced by our simulation: 70% of the molecules accumulate in $N \leqslant 1$ and are essentially in the F_1'' component. This last effect is attributed to the fact that molecules in F_2'' can be excited by both $^{O}P_{12}$ and $^{P}Q_{12}$ for which the sum of the Hönl–London factors is roughly three times larger as the Hönl–London factor of the $^{P}P_{11}$ that only excites the molecules in F_1''. Given that the decay from the excited state repopulates the components F_1'' and F_2'' equivalently, the net result is an accumulation of molecules in the states of type F_1''. We now can wonder why the pumping process leaves about 30% of the molecules in states $N'' > 1$. Our simulation indicates that this limitation is simply due to an insufficient number of excitations. We found that doubling this number leads to halving the number of molecules in $N'' > 1$.

Finally, we also examined the role of laser polarization and (magnetic field) quantization axis that can produce dark states. For instance, with a circular polarization and a quantization axis on the light propagation axis, the P transitions have dark states $M_J'' = \pm J''$ that cannot be excited by the light field (M_J'' being the projection of J'' on the quantization axis) [31]. Indeed, in such a configuration, we found that the rotational pumping is much less efficient than in the experiment, leaving about 60% of the molecules in $N'' > 1$, essentially in the states F_1'' and, as expected, in $(J'', M_J'' = \pm J'')$ for any value of J''. However in our experiment the magnetic field is not along the laser propagation axis and the good agreement between the experience and our incoherent rate equation model tends to indicate that if coherent (superposition) dark states theoretically exist, they do not seem to play a significant role, probably because the superpositions are destabilized by field fluctuations.

5. Conclusion

In summary, we have demonstrated that two broadband optical sources with proper frequency shaping can achieve an efficient rotational pumping on a cold beam of BaF molecules. Indeed, starting from a rotational temperature of 12 K, typical for this kind of experiment, we managed to accumulate in 440 μs about 70% of the molecules in the two lowest rotational energy levels which corresponds, roughly, to a temperature of 0.8 K. Alternatively, it can be said that the sole rotational pumping leads to increase the populations in $N'' = 0$ and $N'' = 1$ by a factor 14 and 7 respectively (the increase of the total population in $N'' = 0$ and $N'' = 1$ is about 9). Because molecules lying in $v'' = 1$ initially (about 60% of the population in $v'' = 0$) are transferred to $v'' = 0$, these number must be multiplied by 1.6 to account for the real increase in our experiment. Compared to our previous work, the gain in efficiency is directly attributed to an improved resolution of the spectral cut-off (0.27 cm^{-1} versus 4.5 cm^{-1}), now of the same order of magnitude as the separation between the relevant rotational transitions (0.1 cm^{-1}). Our data analysis shows that pumping tends to favor the accumulation in rotational states of the spin component F_1'' which results from the difference in the excitation probabilities of the two spin components. Consistently with the selection rules, the experiment showed that the molecules must occupy at least two rotational levels with different parities. To go further and populate a single rotational level, it may be envisaged to induce purely rotational transitions by means of a microwave field.

In conclusion, we believe that optical pumping should be envisioned as an effective tool for manipulating molecules. Obviously, applied to the current coldest BaF sources, the gain in brightness would be modestly increased by a factor between two and four. However, it should also be considered that optical pumping relaxes constraints on cold molecule production techniques. For example, if we assume that a cold source can deliver a larger number of molecules at the cost of a too important increase of its rotational temperature, a compensation of this increase is accessible by rotational pumping.

Acknowledgments

This work was supported by the ANR MolSisCool project and the Dim Nano-K CPMV project.

Data availability statement

The data that support the findings of this study are available upon reasonable request from the authors.

ORCID iDs

D Comparat https://orcid.org/0000-0001-5884-2882
H Lignier https://orcid.org/0000-0002-8347-2390

References

[1] Carr L D, DeMille D, Krems R V and Ye J 2009 *New J. Phys.* **11** 055049
[2] Barry J F, Shuman E S and DeMille D 2011 *Phys. Chem. Chem. Phys.* **13** 18936
[3] Aggarwal P *et al* 2018 *Eur. Phys. J.* D **72** 197
[4] Altuntas E, Ammon J, Cahn S B and Demille D 2018 *Phys. Rev. Lett.* **120** 142501
[5] Kogel F, Rockenhäuser M, Albrecht R and Langen T 2021 *New J. Phys.* **23** 095003
[6] Albrecht R, Scharwaechter M, Sixt T, Hofer L and Langen T 2020 *Phys. Rev.* A **101** 013413
[7] Aggarwal P *et al* 2021 *Rev. Sci. Instrum.* **92** 033202
[8] Barry J F, McCarron D J, Norrgard E B, Steinecker M H and Demille D 2014 *Nature* **512** 286
[9] Truppe S, Williams H J, Hambach M, Caldwell L, Fitch N J, Hinds E A, Sauer B E and Tarbutt M R 2017 *Nat. Phys.* **13** 1173
[10] Chen T, Bu W and Yan B 2017 *Phys. Rev.* A **96** 053401
[11] Hao Y *et al* 2019 *J. Chem. Phys.* **151** 034302
[12] Jadbabaie A, Pilgram N H, Klos J, Kotochigova S and Hutzler N R 2020 *New J. Phys.* **22** 22002
[13] Fitch N J and Tarbutt M R 2016 *ChemPhysChem* **17** 3609
[14] DeMille D, Doyle J M and Sushkov A O 2017 Probing the frontiers of particle physics with tabletop-scale experiments *Science* **357** 990–4
[15] Schneider T, Roth B, Duncker H, Ernsting I and Schiller S 2010 *Nat. Phys.* **6** 275
[16] Wakim A, Zabawa P, Haruza M and Bigelow N P 2012 *Opt. Express* **20** 16083–91
[17] Manai I, Horchani R, Lignier H, Pillet P, Comparat D, Fioretti A and Allegrini M 2012 *Phys. Rev. Lett.* **109** 183001
[18] Cournol A, Pillet P, Lignier H and Comparat D 2018 *Phys. Rev.* A **97** 031401
[19] Stollenwerk P R, Antonov I O, Venkataramanababu S, Lin Y-W and Odom B C 2020 *Phys. Rev. Lett.* **125** 113201
[20] Fitch N J and Tarbutt M R 2021 *Adv. At. Mol. Opt. Phys.* **70** 157
[21] Courageux T, Cournol A, Comparat D, Viaris De Lesegno B and Lignier H 2020 *Phys. Chem. Chem. Phys.* **22** 19864
[22] Wall T E and Phys J 2016 *J. Phys. B: At. Mol. Opt. Phys.* **49** 243001
[23] Monmayrant A, Weber S and Chatel B 2010 *J. Phys. B: At. Mol. Opt. Phys.* **43** 103001
[24] Aggarwal P *et al* 2019 *Phys. Rev.* A **100** 052503
[25] Effantin C, Bernard A, d'Incan J, Wannous G, Vergès J and Barrow R F 1990 *Mol. Phys.* **70** 735
[26] Western C M 2017 PGOPHER: a program for simulating rotational, vibrational and electronic spectra *J. Quant. Spectrosc. Radiat. Transfer* **186** 221–42
[27] Aoiz F J, Díez-Rojo T, Herrero V J, Martínez-Haya B, Menéndez M, Quintana P, Ramonat L, Tanarro I and Verdasco E 1999 *J. Phys. Chem* A **103** 823
[28] Mori H, Niimi T, Akiyama I and Tsuzuki T 2005 *Phys. Fluids* **17** 117103
[29] Steimle T C, Frey S, Le A, Demille D, Rahmlow D A and Linton C 2011 *Phys. Rev.* A **84** 012508
[30] Comparat D 2020 dcompara/laser-interaction-in-fields-rate-equations-forces: C++ code for laser interaction and forces *GitHub repository* https://github.com/dcompara/Laser-interaction-in-fields-rate-equations-forces
[31] Cournol A, Pillet P, Lignier H and Comparat D 2016 *Phys. Rev.* A **93** 053423